Order online now!

www.rockland.com
tech@rockland.com
+1 484.791.3823

Datasheet for 200-4136S

Beta Galactosidase Antibody

Overview

Description:	Anti-Beta Galactosidase (E. coli) (RABBIT) Antibody - 200-4136S
Item No.:	200-4136S
Size:	25 µL
Applications:	ELISA, WB, IF, IHC, Multiplex
Reactivity:	b-GAL
Host Species:	Rabbit

Product Details

Background:	Anti Beta Galactosidase Antibody recognizes the enzyme beta galactosidase, or β-galactosidase, that is a component of assays used frequently in genetics, molecular biology (see X-gal) for a blue white screen, and other life sciences. IPTG induces production of β-galactosidase by binding and inhibiting the lac repressor. Since it is highly expressed and accumulated in lysosomes in senescent cells, it is used as a senescence biomarker both in vivo and in vitro in qualitative and quantitative assays, despite its limitations. Anti-beta Galactosidase Antibody is ideal for investigators involved in enzyme research.
Synonyms:	rabbit anti-Beta Galactosidase Antibody, rabbit anti-beta gal antibody, ß-Gal, Anti-ß-Gal Antibody
Host Species:	Rabbit
Clonality:	Polyclonal
Format:	IgG

Target Details

Gene Name:	lacZ
Reactivity:	b-GAL
Immunogen Type:	Native Protein
Immunogen:	Full length native Beta Galactosidase isolated from E.coli

Purity/Specificity:	Beta-Galactosidase Antibody is an IgG fraction antibody purified from monospecific antiserum by a multi-step process which includes delipidation, salt fractionation and ion exchange chromatography followed by extensive dialysis against the buffer stated above. Assay by immunoelectrophoresis resulted in a single precipitin arc against anti-Rabbit Serum as well as purified and partially purified Beta Galactosidase [E.coli]. Cross reactivity against Beta Galactosidase from other tissues and species may occur but have not been specifically determined. Very low background staining has been reported in various assays.
Relevant Links:	• NCBI - NP_414878.1 • UniProtKB - P00722

Application Details

Tested Applications:	ELISA, WB
Suggested Applications:	IF, IHC, Multiplex (Based on references)
Application Note:	Anti-Beta-Gal Antibody has been tested by ELISA and western blot and is suitable for dot blot, immunofluorescence microscopy, immunoprecipitation, conjugation and most immunological methods requiring high titer and specificity. The antibody recognizes both frozen tissue sections, paraffin embedded tissue and 4% paraformaldehyde fixed tissue for most immunohistochemical analysis. A 1:1,500 dilution has been reported to detect beta-galactosidase in adult rat spinal cord tissue after infection with helper-dependent adenovirus expressing lacZ. In this particular experiment, tissue was perfused with 4% paraformaldehyde and cryostat-cut (35 µm) to produce free-floating sections.
Assay Dilutions:	All assays should be optimized by the user. Recommended dilutions (if any) may be listed below.
ELISA:	1:10,000
IF:	User Optimized
IHC:	1:1,500
WB:	1:5,000 - 1:10,000

Formulation

Physical State:	Liquid (sterile filtered)
Concentration:	1.04 mg/mL by UV absorbance at 280 nm
Buffer:	0.02 M Potassium Phosphate, 0.15 M Sodium Chloride, pH 7.2
Preservative:	0.01% (w/v) Sodium Azide
Stabilizer:	None

Shipping & Handling

Shipping Condition:	Dry Ice
Storage Condition:	Store vial at -20° C or below prior to opening. This vial contains a relatively low volume of reagent (25 µL). To minimize loss of volume dilute 1:10 by adding 225 µL of the buffer stated above directly to the vial. Recap, mix thoroughly and briefly centrifuge to collect the volume at the bottom of the vial. Use this intermediate dilution when calculating final dilutions as recommended below. Store the vial at -20°C or below after dilution. Avoid cycles of freezing and thawing.
Expiration:	Expiration date is one (1) year from date of receipt.

Images

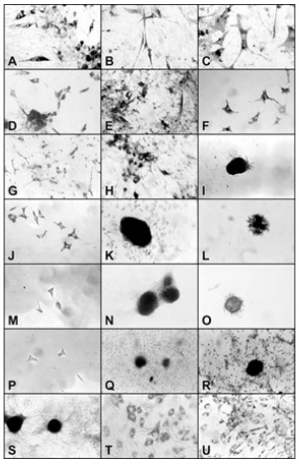

Immunofluorescence Microscopy
Rat-A2B2 incubated for one week (A, G, H, and J), two weeks (B–F, M, O, P, T, and U), four weeks (N and Q), six weeks (I, K, R, and S), or eight weeks (L) in TM and 10–8 M Dex (A–L, T, and U) or TM and 10–7 M Dex (M–S). Photographed with brightfield microscopy; original magnifications, ×200 (A, C, F, H, J, M, P, and T), ×100 (B, D, E, and G), or ×40 (I, K, L, N, O, Q–S, and U). A: Mononucleated cells showing heavy intracellular staining for myogenin (F5D). B: Mononucleated and binucleated cells showing moderate to heavy intracellular staining for sarcomeric myosin (MF-20). C: Mononucleated and binucleated cells showing moderate to heavy intracellular staining for antiskeletal muscle fast myosin (MY-32). D: Mononucleated cells showing moderate to heavy intracellular staining for skeletal myosin heavy chain (ALD58). E: Mononucleated and binucleated cells showing heavy intracellular staining for skeletal myosin fast chain (A4.74). F: Mononucleated cells showing heavy intracellular staining for smooth muscle α-actin (IA4). G: Mononucleated cells showing moderate intracellular staining for cardiotin (cardiac myocytes, MAB 3252). H: Mononucleated cells demonstrating heavy intracellular staining for bone sialoprotein II (WV1D1). I: Nodule of cells demonstrating extracellular staining for bone sialoprotein II (WV1D1). J: Mononucleated cells demonstrating moderate to heavy intracellular staining for osteopontine (MP111). K: Nodule of cells demonstrating extracellular staining for osteopontine (MP111). L: Nodule of cells demonstrating extracellular staining for calcium phosphate using the von Kossa procedure

(vK). M: Mononucleated cells with intracellular staining for cartilage-specific collagen pro type-II (CIIC1). N: Three nodules demonstrating intense extracellular staining for cartilage-specific collagen pro type-II (CIIC1). O: Single nodule of cells demonstrating moderate extracellular staining for cartilage-specific collagen type-II (HC-II). P: Mononucleated cells demonstrating moderate intracellular staining for cartilage-specific collagen type-IX (D1-9). Q: Three nodules demonstrating extracellular staining for sulfated glycosaminoglycan chains of proteoglycans (Perfix/Alcec Blue). R: Nodule demonstrating extracellular staining for sulfated glycosaminoglycan chains of proteoglycans (Safranin-O, pH 1.0). Individual nuclei stained with antibody to β-galactosidase (Gal-19) [p/n 200-4136] and visualized with 3-3'-diaminobenzidine (DAB). S: Two nodules demonstrating extracellular staining for sulfated glycosaminoglycan chains of proteoglycans (Alcian Blue, pH 1.0). T: Mononucleated cells with moderate to heavily stained intracellular vesicles demonstrating saturated neutral lipids (Oil Red-O), indicative of adipocytes. U: Mononucleated cells with moderate to intensely stained intracellular vesicles demonstrating saturated neutral lipids (Sudan Black-B), indicative of adipocytes. Fig 3. PMID: 14983513

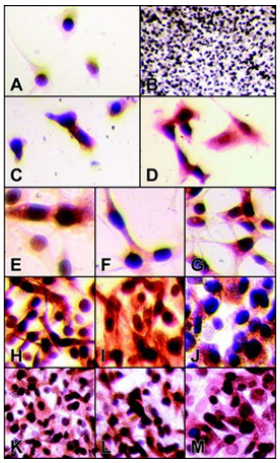

Immunofluorescence Microscopy
Scl-40β clone incubated with antibody to β-galactosidase to demonstrate nuclear LacZ-transfected gene expression and stained with DAB (dark purple/black), then incubated with antibody to specific phenotypic expression markers, as noted, and counterstained with 3-amino-9-ethylcarbazole (AEC) (red/orange). Embryonic-like: Scl-40β grown in serum-free medium containing 2 µg/ml insulin (C and D). Ectodermal: Scl-40β grown for one week in serum-free medium containing 2 µg/ml insulin, 10–6 M dexamethasone, 1% SS12 at pH 7.4 to induce ectodermal lineage cells (E–G). Mesodermal: Scl-40β grown for one week in serum-free medium containing 2 µg/ml insulin, 10–6 M dexamethasone, 1% SS9 at pH 7.4 to induce mesodermal lineage cells (H–J). Endodermal: Scl-40β grown for one week in serum-free medium containing 2 µg/ml insulin, 10–6 M dexamethasone, 15% SS12 at pH 7.6 to induce endodermal lineage cells (K–M). Original magnifications, ×300 (A, C–J, and M), ×200 (K and L), ×100 (B). A: Scl-40β grown for one week in serum-free medium containing 2 µg/ml insulin. Note widely dispersed mononucleated cells with no apparent cellular proliferation or cell degeneration during culture period. B: Scl-40β grown for one week in serum-free medium with serum containing PDGF-like (proliferative) and ADF-like (antidifferentiative/inhibitory) activities. Note multiple confluent layers of cells expressing nuclear β-galactosidase expression. C: MC-813-70, antibody to stage-specific embryonic antigen-4 (Lannagi et al., 1983). D: CEA-CAM-1, antibody to CEA-CAM-1 (Hixson) (Estrera et al., 1999). E: MAB353, antibody to nestin for the identification of neurogenic progenitor cells (Gritti et al., 1996). F: SV2, antibody to synaptic vesicles (Feany et al., 1992). G: Rip, antibody to oligodendrocytes (Friedman et al., 1989). H: MF-20, antibody to sarcomeric myosin (Bader et al., 1982). I: HC-II, antibody to type-II collagen (Burgeson and Hollister, 1979; Kumagai et al., 1994). J: WV1D1, antibody to bone sialoprotein II (Kasugai et al., 1992). K: R-AFP, antibody to rat-specific AFP (Mujoo et al., 1983). L: YM-PS5088, antibody to insulin-secreting β-cells (Young, 2003; Young et al., 2003). M: OC4, antibody to liver progenitor cells, biliary epithelial cells, oval cells, and canalicular cells (Hixson et al., 1984, 1990, 2000; Walborg et al., 1985; Faris et al., 1991; Gordon et al., 2000). Fig 6. PMID: 14983513

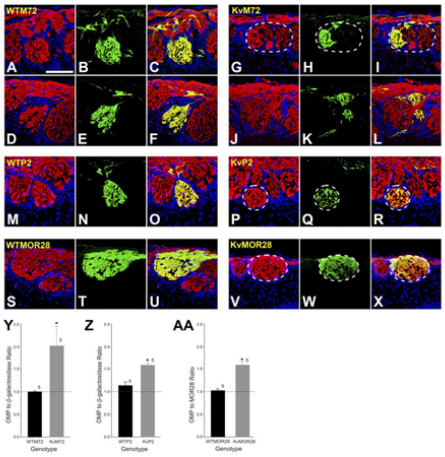

Immunofluorescence Microscopy
Absence of Kv1.3 ion channel induces the development of heterogeneous glomeruli. A–L: Representative two-photon confocal micrographs of WTM72 (left panels; A–F) and KvM72 glomeruli (right panels; G–L). A,D,G,J: Red channel; sections were processed for olfactory marker protein (OMP; 1:1,000) immunocytochemistry to visualize axons projecting from all mature OSNs. B,E,H,K: Green channel; sections were processed for β-galactosidase immunocytochemistry (1:1,000). C,F,I,L: Merged image, yellow. Note the incomplete innervation of the M72 glomerulus (I,L) in KvM72 as evidenced by red only fibers creating a heterogeneous M72 glomerulus. Postnatal day 20. M–R: Representative two-photon confocal micrograph of a WTP2 (M–O) and a KvP2 glomerulus (P–R). Red channel represents OMP; green, β-galactosidase; yellow, merged image. Note the presence of a heterogeneous P2 glomerulus (R) in the KvP2 mouse. A few OMP-positive, β-galactosidase-negative fibers are also visible in WTP2 mice (O). S–X: Representative two-photon confocal micrograph of a WTMOR28 (S-U) and a Kv-MOR28 glomerulus (V–X). Red channel represents OMP; green, MOR28 immunoreactivity; yellow, merged image. KvMOR28 mice exhibit heterogeneous glomeruli (X). Y: Histogram plot of αOMP to α-β-galactosidase pixel density for M72 glomeruli of WTM72 and KvM72 mice. A ratio of 1.0 represents complete overlapping of OMP and β-galactosidase-immunoreactive axons (homogeneous glomerulus), whereas a ratio > 1.0 represents more OMP-immunoreactive axons (heterogeneous glomeruli). Values are mean ± SEM. *, significantly different by Student's t-test, $p \leq 0.05$. Z: Same as Y but for WTP2 and KvP2. AA: Histogram plot of αOMP to αMOR28 pixel density for MOR28 glomeruli of WTMOR28 vs. KvMOR28 mice. Values are mean ± SEM. *, significantly different by Student's t-test, $p \leq 0.05$. Scale bar = 100 µm in A (applies to A–X). Fig 5. PMID: 18022950

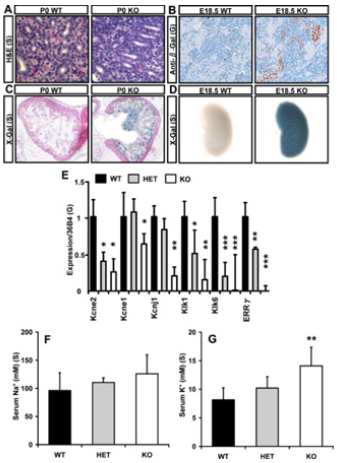

Immunofluorescence Microscopy
Loss of ERRγ alters renal markers. A, Hematoxylin and eosin staining of kidney does not reveal significant differences in ERRγ null mice. B, Anti-β-galactosidase staining indicates ERRγ expression in the distal tubules. C, X-gal staining of frozen sections shows that ERRγ is expressed in the distal tubules and collecting ducts of the kidney. D, Whole-mount X-gal staining reveals the high expression of ERRγ throughout the cortex of the kidney. E, In kidney, loss of ERRγ produces a down-regulation of potassium channels and components of the KSS as detected by triplicate quantitative PCR (n = 3 WT; 9 HET; 6 KO). F, Serum sodium levels did not increase to statistically significant degree in ERRγ null mice at E18.5. G, Serum potassium levels were increased by more than 70% in ERRγ null animals at E18.5. Values ± sd; *, P < 0.05; **, P < 0.01; ***, P < 0.001 by two-tailed Student's t test. S, Salk mice; G, GlaxoSmithKline mice; H&E, hematoxylin and eosin; HET, heterozygous. Fig 5.
PMID: 19965931

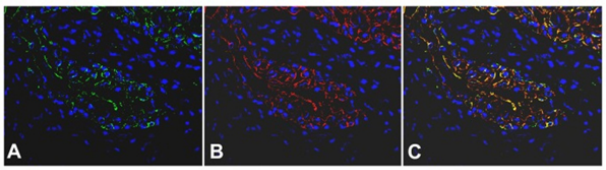

Immunofluorescence Microscopy
Immunofluorescent staining of β-galactosideasae and cytokeratin expression of urinary bladder after intravesical treatment with Adeno-Cre. Adeno-Cre (8.46×108 pfu per mouse) was delivered into the bladder lumen of ROSA mice for 2 hours (n=5). Mice were sacrificed and their bladders were removed and processed for immunofluorescence staining. The urothelial mucosa shows in green β-galactosidase (A) and in red cytokeratin 7 expressions (B). In Figure (C), overlapping of the fields (A) and (B) demonstrates the co-localization of β-galactosidase and cytokeratin 7 expressions (orange-yellow). Nuclei were stained with DAPI (blue color). β-galactosidase expression is scattered and observed mainly in the 2/3 upper (inner) layer of the urothelium versus cytokeratin expression which is evenly present in the full thickness of the urothelium. Fig 3.
PMID: 24058630

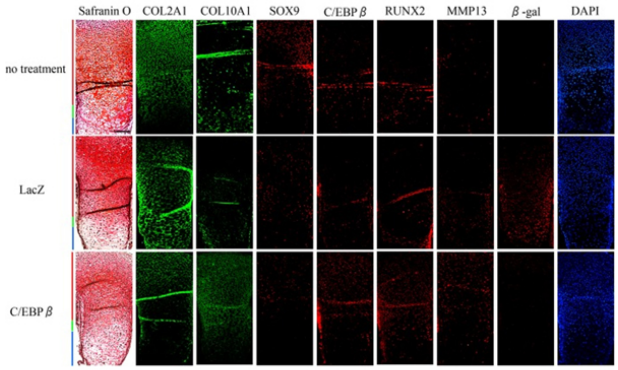

Immunofluorescence Microscopy
C/EBPβ repressed the expression of COL2A1 and SOX9 in ex vivo organ cultures. Ex vivo organ culture of tibias dissected from E14.5 mouse embryos are shown. Tibias were cultured for 4 days without adenovirus vectors (top row) or after transfection with adenovirus vectors expressing LacZ control (middle row) or C/EBPβ (bottom row). Safranin O staining and immunofluorescent staining were performed to localize COL2A1, COL10A1, SOX9, C/EBPβ, RUNX2, and MMP13. β-Galactosidase antibody (β-gal) was used to confirm the transfection efficiency of adenovirus vectors. DAPI was used as a counterstain. Red, green, and blue bars indicate the proliferative, prehypertrophic, and hypertrophic zones, respectively. Scale bar, 500 µm. Histological analysis was repeated at least twice for each sample from six pairs of limbs, respectively. Fig 7.
PMID: 24344131

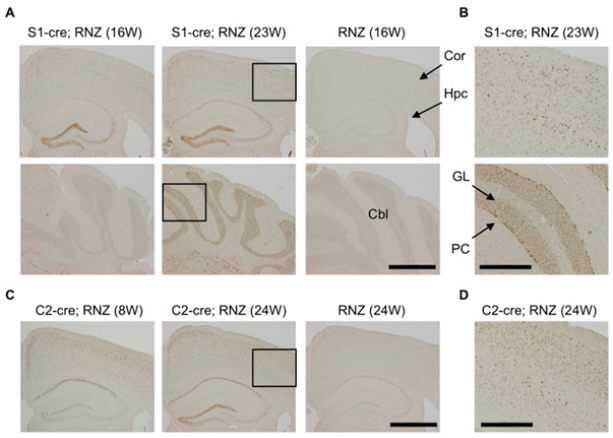

Immunohistochemistry
Transgenic mice for synapsinI-cre (S1-cre) or camk2a-cre (C2-cre) were crossed with RNZ mice. RNZ male mice harboring S1-cre or C2-cre at indicated weeks of age were subjected to anti-LacZ staining to detect cre-mediated DNA recombination. RNZ mice without a cre transgene were used as controls. (A) In S1-cre; RNZ mice at 16 weeks of age, LacZ-positive cells were strongly detected in dentate gyrus and CA3 in hippocampus and some cortical cells, but very few were seen in cerebellum. At 23 weeks, LacZ expression became wider in the cortex and hippocampus, and was clearly detected in cerebellum. No distinct LacZ expression was detected in the control RNZ mice. (B) High magnification of boxed region in (A). LacZ expression was broadly detected in multiple layers of cortex and Purkinje and granular cells of cerebellum in 23 week-old S1-cre; RNZ mice. (C) LacZ-positive cells were broadly detected in brains of 8-week-old C2-cre; RNZ mice, especially in layer II/III of cortex and CA1 of hippocampus. It became wider at 24 weeks of age. Again, no distinct LacZ expression was observed in the control RNZ mice. (D) High magnification of boxed region in (C), indicating detection of LacZ-positive cells in multiple layers of cortex in 24 week-old C2-cre; RNZ mice. Cor (cortex), Hpc (hippocampus), Cbl (cerebellum), PC (Purkinje cell) and GL (granular layer). Bars are 1 mm (A, C) and 0.4 mm (B, D). Fig 1. PMID: 24391875

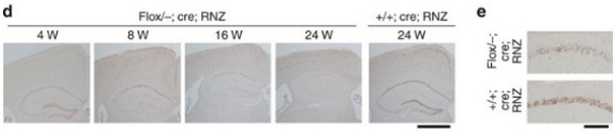

Immunohistochemistry
(d) Anti-LacZ staining of coronal sections of RNZ reporter mice harbouring NF-YA flox/−; cre or +/+; cre at indicated weeks of age. (e) Anti-LacZ-stained CA1 regions of 8-week-old mice. Fig 1. PMID: 24566496

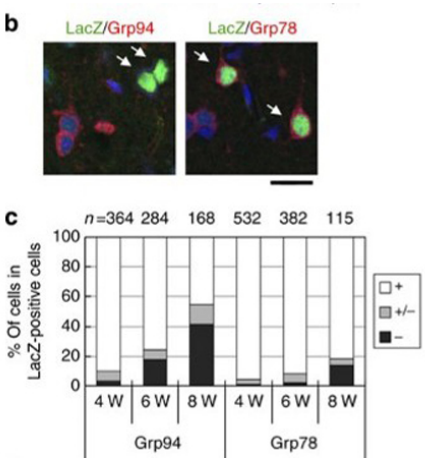

Immunofluorescence Microscopy
(b,c) Coronal sections of RNZ reporter mice harbouring NF-YA flox/−; cre were stained with anti-LacZ together with antibodies for Grp94 or Grp78. (b) Confocal images for cortical region of 8-week-old mice. LacZ-positive cells are indicated by arrows. (c) LacZ-positive cells in cortex region were first picked up and then categorized into three groups based on the staining of Grp94 or Grp78; no signal (−), background level (±) or similar to control level (+). Ratios to total LacZ-positive cells are shown (n means number of analysed cells). Fig 6. PMID: 24566496

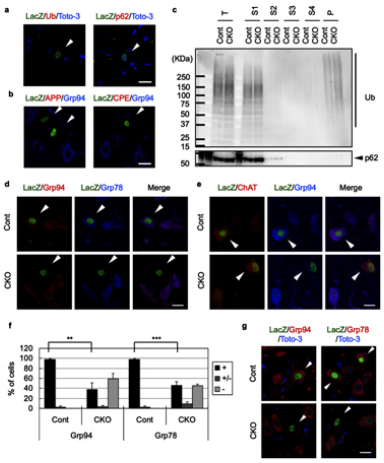

Immunofluorescence Microscopy
(a,b) Cervical cord sections of 6-week-old NF-YA v-cko mice (flox/flox; VA-cre; RNZ) were stained with LacZ together with indicated antibodies. Nuclei were stained with Toto-3 for (a). LacZ-positive cells are indicated by arrowheads. Note no accumulation of Ub, p62, APP or CPE in NF-YA v-cko motor neurons. (c) Isolated spinal cords from 14-week-old NF-YA v-cko mice (flox/flox; VA-cre) and control mice (flox/+) were homogenized (T), and then sequentially solubilized with buffer containing 1% TritonX-100 (S1), DNaseI/RNaseA (S2), 1% Sarkosyl (S3) or 4% Sarkosyl (S4), or with formic acid (P), and then analyzed by western blotting. Note no accumulation of insoluble Ub or p62 in NF-YA v-cko spinal cords. (d,e) Cervical cord sections of 6-week-old NF-YA v-cko (flox/flox; VA-cre; RNZ) or control (flox/+; VA-cre, RNZ) mice were stained with LacZ together with indicated antibodies. LacZ-positive cells are indicated by arrowheads. (d) Loss of both Grp94 and Grp78 in NF-YA v-cko neurons. (e) Remaining ChAT expression in the NF-YA v-cko neurons without Grp94 expression. (f) The LacZ-positive cells were categorized into three groups based on the staining of Grp94 or Grp78; no signal (−), background level (+/−) or similar to the control level (+). Ratios to total counted cells are shown. Values are means + s.d. of four mice data (**P < 0.01, ***P < 0.001, t-test). (g) Facial nuclei of the mice used in a were stained with LacZ together with Grp94 or Grp78. Nuclei were stained with Toto-3. Loss of these ER chaperones in NF-YA v-cko facial motor neurons. Scale bars are 20 µm. Fig 2.
PMID: 27687130

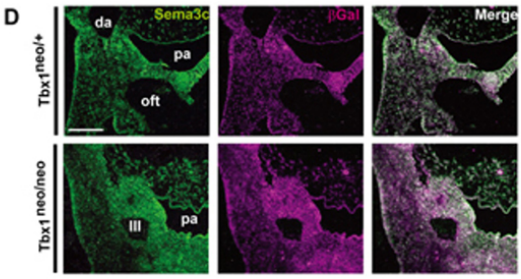

Immunofluorescence Microscopy
(D) Immunostaining for Sema3c (green) and βGal (red) on coronal sections of the pharyngeal arch region in Sema3c int1/3'-lacZ tg:Tbx1 neo/+ or Sema3c int1/3'-lacZ tg:Tbx1 neo/neo embryos. Scale bars, 100 µm. Fig 2.
PMID: 28754980

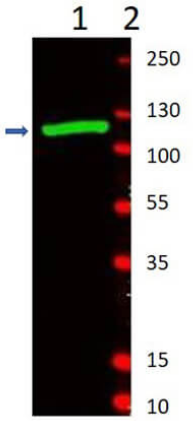

Western Blot
Western Blot of Rabbit Anti-Beta-Galactosidase Antibody. Lane 1: partially purified preparation b-Galactosidase [1.0µg]. Lane 2: Molecular Weight Marker. Primary Antibody: Anti-Beta-Galactosidase at 1:1000 overnight at 2-8°C. Secondary Antibody: Goat Anti-Rabbit IgG IRDye®800 (p/n 611-132-122) 1:10,000 for 45min at RT. Observed MW: ~117kDa.

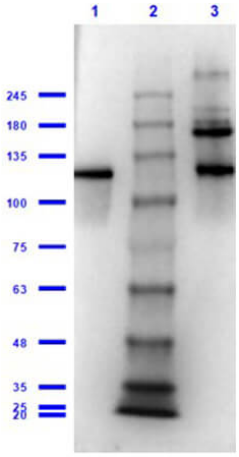

Western Blot
Western Blot of Rabbit Anti-Beta-Galactosidase Antibody. Lane 1: Beta-Galactosidase Reduced [0.1µg]. Lane 2: Opal Prestained Molecular Weight Marker (p/n MB-210-0500). Lane 3: Beta-Galactosidase Non-Reduced [0.1µg]. Primary Antibody: Anti-Beta-Galactosidase at 1:1000 overnight at 2-8°C. Secondary Antibody: Goat Anti-Rabbit IgG HRP (p/n 611 -103-122) 1:70,000 for 30min at RT. Expected MW: ~117kDa.

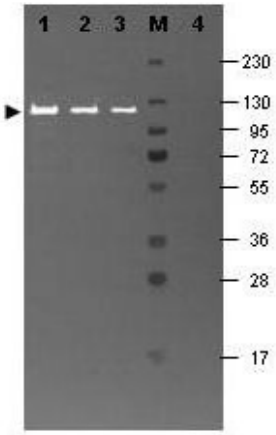

Western Blot
Western blotting using Rockland's Fluorescein conjugated anti-b-Galactosidase antibody shows a band at ~117 kDa (lanes 1 - 3) corresponding to 60 ng, 30 ng and 15 ng, respectively of b-Gal present in partially purified preparations (arrowhead). Lane 4 shows no cross reactivity with proteins present in a non-specific control E.coli lysate. Proteins were resolved on a 4-20% Tris-Glycine gel by SDS-PAGE and transferred to nitrocellulose and blocking using Blocking Buffer for Fluorescent Western Blotting (p/n MB-070). The membrane was probed with fluorescein conjugated anti-b-Galactosidase (p/n 200-4236) diluted to 1:10,000. Reaction occurred for 2 hours at room temperature. Molecular weight estimation was made by comparison to a prestained MW marker in lane M. Fluorescence image was captured using the VersaDoc® Imaging System developed by BIO-RAD. Other detection systems will yield similar results

References

- Krolewski RC et al. A Group of olfactory Receptor Alleles that encode full Length proteins are Down-Regulated as olfactory Sensory neurons Mature. *Sci Rep.* (2020)
- Pfannenstiel SC. et al. Hearing Preservation Following Repeated Adenovector Delivery. *Anat Rec (Hoboken).* (2020)
- El Agha E, Moiseenko A, Kheirollahi V, et al. Two-Way Conversion between Lipogenic and Myogenic Fibroblastic Phenotypes Marks the Progression and Resolution of Lung Fibrosis *Cell Stem Cell.* (2017)
- Kodo K et al. Regulation of Sema3c and the interaction between cardiac neural crest and second heart field during outflow tract development. *Sci Rep.* (2017)
- Yamanaka T et al. Differential roles of NF-Y transcription factor in ER chaperone expression and neuronal maintenance in the CNS. *Sci Rep.* (2016)
- Yamanaka T et al. NF-Y inactivation causes atypical neurodegeneration characterized by ubiquitin and p62 accumulation and endoplasmic reticulum disorganization. *Nat Commun.* (2014)
- Van Batavia J et al. Bladder cancers arise from distinct urothelial sub-populations. *Nat Cell Biol.* (2014)
- Ushijima T et al. CCAAT/enhancer-binding protein β regulates the repression of type II collagen expression during the differentiation from proliferative to hypertrophic chondrocytes. *J Biol Chem* (2014)
- Yamanaka T et al. Loss of aPKCλ in differentiated neurons disrupts the polarity complex but does not induce obvious neuronal loss or disorientation in mouse brains. *PLoS One* (2013)
- Yang X. et al. Simultaneous activation of Kras and inactivation of p53 induces soft tissue sarcoma and bladder urothelial hyperplasia. *PLoS One* (2013)
- Hubener J et al. N-terminal ataxin-3 causes neurological symptoms with inclusions, endoplasmic reticulum stress and ribosomal dislocation. *Brain.* (2011)
- Alaynick WA et al. ERRγ regulates cardiac, gastric, and renal potassium homeostasis. *Mol Endocrinol.* (2009)
- Biju KC et al. Deletion of voltage-gated channel affects glomerular refinement and odorant receptor expression in the mouse olfactory system. *J Comp Neurol.* (2008)
- Hayworth CR et al. Induction of neuregulin signaling in mouse schwann cells in vivo mimics responses to denervation. *J Neurosci* (2006)
- Nguyen HG et al. Conditional overexpression of transgenes in megakaryocytes and platelets in vivo. *Blood* (2005)
- Dufresne-Martin G et al. Peptide mass fingerprinting by matrix-assisted laser desorption ionization mass spectrometry of proteins detected by immunostaining on nitrocellulose. *Proteomics.* (2005)
- Young HE et al. Clonogenic analysis reveals reserve stem cells in postnatal mammals. II. Pluripotent epiblastic-like stem cells. *Anat Rec A Discov Mol Cell Evol Biol.* (2004)

Disclaimer

This product is for research use only and is not intended for therapeutic or diagnostic applications. Please contact a technical service representative for more information. All products of animal origin manufactured by Rockland Immunochemicals are derived from starting materials of North American origin. Collection was performed in United States Department of Agriculture (USDA) inspected facilities and all materials have been inspected and certified to be free of disease and suitable for exportation. All properties listed are typical characteristics and are not specifications. All suggestions and data are offered in good faith but without guarantee as conditions and methods of use of our products are beyond our control. All claims must be made within 30 days following the date of delivery. The prospective user must determine the suitability of our materials before adopting them on a commercial scale. Suggested uses of our products are not recommendations to use our products in violation of any patent or as a license under any patent of Rockland Immunochemicals, Inc. If you require a commercial license to use this material and do not have one, then return this material, unopened to: Rockland Inc., P.O. BOX 5199, Limerick, Pennsylvania, USA.